Modelling of Liquid/Liquid Interface Movement during Spindle Rotation of Refractory - Slag Corrosion Test

H Lee[1], B Choi[2] and Y Chung[3*]

1. PhD student, Department of advanced materials of engineering, Tech University of Korea, 237, Sangidaehak-ro, Shiheung-si 15073, Republic of Korea. Email: rlghkemd369@tukorea.ac.kr
2. Senior research engineer, Hyundai steel, 1480, Bukbusaneop-ro, Songak-Eup, Chungnam, 31719, Republic of Korea. Email: bkchoi@hyundai-steel.com
3. Professor, Department of advanced materials of engineering, Tech University of Korea, 237, Sangidaehak-ro, Shiheung-si 15073, Republic of Korea. Email: ychung@tukorea.ac.kr

Keywords: CFD(Fluent); water model; refractory corrosion; rotor; interface movement

ABSTRACT

Numerous studies have explored refractory corrosion in the presence of slag and/or metal, utilizing the Finger Rotating Test (FRT). Recent experimental results revealed that corrosion initially increased with rising rotation velocity but was then suppressed above a critical rotating speed, under conditions involving a two-liquid solution of slag and molten steel. This phenomenon indicated that the liquid/liquid interface movement occurred during spindle rotor. However, understanding of the phenomenon, known as the rod climbing effect, remains inadequate in the case involving slag, molten steel, and refractories. To gain deeper insights, a simulation experiment was conducted on the phenomenon using silicon oil/water, and the phenomenon was analysed using computerized simulation software (Ansys Fluent). Experimental modelling demonstrated that interfacial movement occurs even at low rotation velocity, as low as 200 rpm, when the viscosity of silicone oil is at 100 cP. Computational analysis utilizing the Volume of Fluid (VOF) method and a realizable k-ε turbulence model elucidated that interface elevation during rotor rotation arises due to viscosity disparities between the two fluids. Furthermore, this movement is more pronounced when the viscosity difference is lower. Additionally, the study findings suggest that higher density differences between two liquids suppress the phenomenon of interface movement.

INTRODUCTION

MgO-C refractories are mainly used as furnace lining materials due to their high mechanical strength, slag corrosion resistance, and thermal shock resistance.[1-2] The furnace lining lifetime is determined by damage to the refractory due to chemical corrosion, thermal shock, and mechanical wear.[3-7] Among these, chemical corrosion by slag is one of the main mechanisms causing serious wear of refractories[8]. To improve the lining lifetime of the furnace, some researchers have studied the corrosion mechanism of MgO-C refractories.[5, 9-12]

Methods for researching corrosion of refractory materials by slag can be divided into static and dynamic methods that embody the flow conditions of actual operation. A representative static method is the cup test, which processes refractory materials into a cup shape, adds solid slag, and observes the reaction after melting.[5,9] Meanwhile, a method of providing slag flow is the rotary slag test, which involves attaching a refractory material to a rotary furnace, putting molten slag in it, and then rotating the furnace to check the corrosion phenomenon.[10] However, FRT, which processes refractory materials into finger shapes and rotates them in molten slag and/or steel in a crucible, is the most widely used.[13,14]
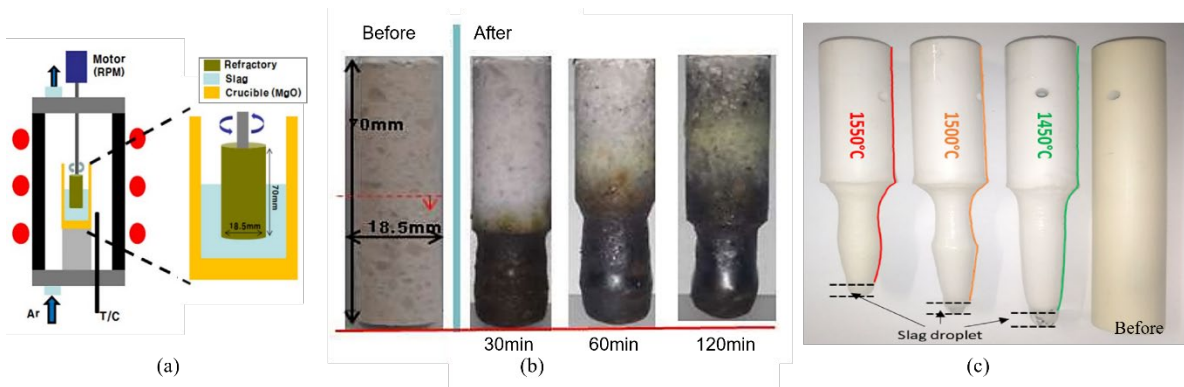
FIG 1 – Examples of FRT studies

Corrosion under operational conditions primarily arises due to the Marangoni effect at the interface between slag and molten steel.[15] Previous research suggests that an increase in rotational speed increases corrosion or reaction rates as a result of the combined effects of forced and Marangoni convection.[16] However, recent findings by Um et al.[17] under a two-liquid solution condition comprising slag and molten steel, revealed that corrosion initially rose with increasing rotation velocity and was suppressed above a critical value.

This observed phenomenon, known as the rod climbing effect (or Weissenberg effect), typically manifests in non-Newtonian fluids.[18] However, recent studies have demonstrated its occurrence in Newtonian fluids under specific circumstances.[19,20] Despite this, research concerning the phenomenon among slag, molten steel, and refractories remains insufficient. To complement this, our study delves into fluid dynamics and influencing factors utilizing a water model and computational fluid dynamics using commercial software Ansys Fluent.

EXPERIEMENTS

Water/silicone oil experimental

Experiments utilizing water/silicone oil were conducted to simulate FRT involving slag and molten steel. Figure 2 depicts a schematic diagram of the simulation apparatus. Each experiment utilized 150 g of silicone oil and water, with a small quantity of red dye added to the water to enhance visibility. The rotating body consisted of MgO-C refractory material, processed to a diameter of 20mm and a length of 50mm, and coupled with a metal rod connected to a motor to induce rotational motion. Transparent glass crucibles (outer diameter 50mm, inner diameter 40mm, height 130mm) with internal monitoring capabilities were utilized. Real-time imaging was recorded by a CCD camera to observe interface movement corresponding to rotation. Experiments were conducted under standard room temperature and atmospheric conditions.

Considering the viscosity effect, silicone oils with varying viscosities (100 cP and 1,000 cP) were employed. The rotational velocity in both conditions was experimentally constrained to the maximum value that preserved the interface between the two fluids without inducing mixing due to rotation. each ranged up to 700 rpm under conditions with 100 cP silicone oil and up to 1,000 rpm under conditions with 1,000 cP silicone oil.
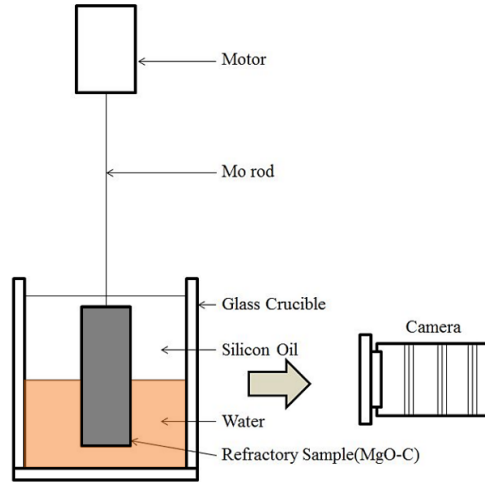
FIG 2 – A schematic of finger rotating test

• Computational Simulation

Ansys Fluent was used for computer simulation. The following assumptions and conditions were used to simulate the phenomenon.

o Fundamental assumption

(1) The fluid is assumed to be an incompressible Newtonian fluid.

(2) The analysis of heat transfer under isothermal conditions is ignored.

(3) Unlike the actual reaction, the slag, molten steel, and refractory material are assumed not to react with each other, so the initial form of the refractory material is maintained. Slag and molten steel are assumed to be in a uniform state, so there is no bias in the physical values.

o Governing equations

The most basic governing equations used in CFD simulations are as follows.

- Continuity equation

$$\frac{\partial \rho}{\partial t} + \nabla \cdot (\rho u) = 0 \text{ ----- (1)}$$

where ρ is fluid density, t is time, u is the flow velocity vector field.

- Momentum equation

$$\frac{\partial \rho u_i}{\partial t} + \frac{\partial}{\partial x_j}\left(\rho u_i u_j\right) = -\frac{\partial p}{\partial x_i} + \frac{\partial \tau_{ij}}{\partial x_j} \text{ ----- (2)}$$

where ρ is fluid density, u is the velocity of fluid, and P is static flow pressure.

The Realized k-ε model[21] was used to accurately simulate the rotation. This model was developed to improve the flow predictions of the standard k-ε model for boundary layer flows, and separated flows, and flows with rotational and vortex characteristics.

- The equation of turbulent kinetic energy (k)

$$\frac{\partial}{\partial t}(\rho k) + \frac{\partial}{\partial x_j}\left(\rho k u_j\right) = \frac{\partial}{\partial x_j}\left[\left(\mu + \frac{\mu_t}{\sigma_k}\right)\frac{\partial k}{\partial x_j}\right] + G_k + G_b - \rho \varepsilon - Y_M + S_k \text{ ----- (3)}$$

- The equation of turbulent kinetic energy dissipation (ε)

$$\frac{\partial}{\partial t}(\rho \varepsilon) + \frac{\partial}{\partial x_j}\left(\rho \varepsilon u_j\right) = \frac{\partial}{\partial x_j}\left[\left(\mu + \frac{\mu_t}{\varepsilon}\right)\frac{\partial \varepsilon}{\partial x_j}\right] + \rho C_1 S_\varepsilon - \rho C_2 \frac{\varepsilon^2}{k+\sqrt{\nu\varepsilon}} + C_{1\varepsilon}\frac{\varepsilon}{k}C_{3\varepsilon}C_b + S_\varepsilon \text{ ----- (4)}$$

where G_k is the generation of turbulence kinetic energy due to the mean velocity gradients, G_b is the generation of turbulence kinetic energy due to buoyancy, Y_M is the contribution of the fluctuating dilatation in compressible turbulence to the overall dissipation rate, σ_k, σ_ε are the turbulent Prandtl numbers for k and ε, respectively, and S_k, S_ε are user-defined source terms.

o **Computational simulation conditions**

To perform a computational simulation of the experiment utilizing water/silicone oil, the physical properties were obtained from the previous water/silicone oil experiment. For the modelling conditions, Volume of Fraction was utilized as a multi-phase condition, and Multiple Reference Frame was employed for rotation, as depicted in Table 1. To reduce computation time, a 2D model was utilized, consisting of 73,236 quadrilateral meshes. The Realizable k-ε model was chosen, and the roughness height was measured and implemented, with the default roughness constant applied. The simulation results were validated against those obtained from the water/silicone oil experiment, confirming the accuracy of the simulation.

Considering the differences in viscosity and density between liquid metal and slag, we investigated interfacial movement by varying the physical properties of silicone oil. Silicone oil viscosity was adjusted to match the experimental conditions, 100 cP and 1,000 cP. Furthermore, density was expressed as a ratio. The density ratio of water to silicone oil set at 0.97 and 0.50, respectively.

TABLE 1 – Physical properties, Operation conditions for FRT computational simulation

Parameter	Value
Physical properties of water	
Density (kg/m^3)	1,000
Viscosity (cP)	1
Physical properties of silicone oil	
Density (kg/m^3)	970
Viscosity (cP)	100/ 1,000
Tensions between the fluids	
Surface tension of water (N/m)	0.061
Surface tension of silicone oil (N/m)	0.024
Interfacial tension between water and silicone oil (N/m)	0.042[22]
Roughness of the MgO-C rotor	
Roughness height (μm)	0.42
Roughness constant	0.5
Operation conditions	
Rotation Speed (rpm)	0 ~ 900
Initial interface height (cm)	4.2

RESULTS AND DISCUSSIONS

Water/silicone oil experimental results

Experimental investigations were conducted using water and silicone oil with viscosities of 100 cP and 1,000 cP, respectively. Figure 3(a) depicts the initial appearance before the experiment, while Figure 3(b) depicts the experimental setup under conditions of 700 rpm and 1,000 cP viscosity of silicone oil. To quantify the displacement of the interface, the height of the three-phase interface is defined ΔH.

$$\Delta H = H_{measured} - H_{inital} \text{ ----- (5)}$$

Figures 3(c) and 3(d) represent the results for silicone oil viscosities of 100 cP and 1,000 cP, respectively. In both cases, an increase in the rotational speed of the refractory material led to an upward movement of the three-phase interface between water, silicone oil, and the refractory material. With 100 cP silicone oil, a gradual change in height was observed from 200 rpm onwards, whereas with 1,000 cP silicone oil, a sharp change in height occurred from 300 rpm onwards. Hence, a smaller difference between the viscosities of silicone oil and water resulted in greater interfacial displacement.

(a)   (b)   (c)   (d)
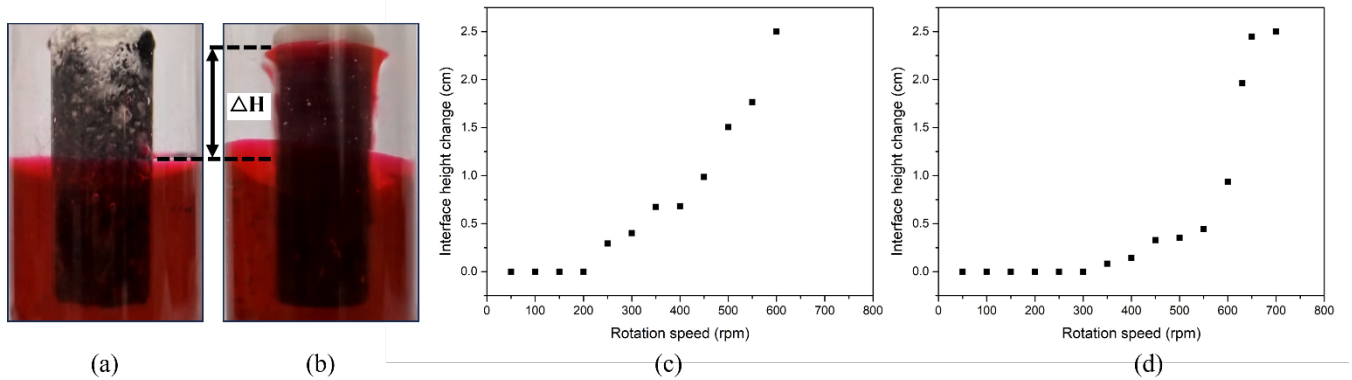
FIG 3 – (a) initial appearance preceding experiment, (b) appearance post-rotation at 700 rpm, (c) plot depicting interface height variation with rotation velocity in water/silicone oil experiment under 100 cP silicone oil condition, (d) under 1,000 cP silicone oil condition.

Computational simulation results

Computational simulations were conducted on water/silicone oil experiment when the viscosity of silicone oil was 100 cP and 1,000 cP. The dataset employed in the computer simulations is outlined in Table 1. Figure 4(a) and (b) present both experimental and simulated data for silicone oil viscosities of 100 cP and 1,000 cP, respectively. In the case of 100 cP, a slight interfacial height change in height was observed even at 75 rpm in the simulation, and a sharp change occurred between 450 rpm and 500rm. Even in the case of 1,000 cP, a slight interfacial movement was observed even below 100 rpm, a phenomenon was not observed in the experimental results. In addition, the difference with the experimental results increased above 800 rpm. Nevertheless, the trend of increasing interface heights with rising rotational speed of the refractory material well simulated that observed in the experiments.

Figure 4(c) illustrates the schematic representation of liquid flow under conditions of 1,000 cP viscosity for silicone oil at 525 rpm. Fluid velocities are depicted using a colour gradient, where red indicates high velocity and blue represents low velocity. Near the rotating body, silicone oil has high fluid velocities, while other regions experience relative stagnation. Conversely, water has slower fluid velocities near the rotor, with convection flow around it. As water flows move the interface near the rotating body, the silicone oil-water interface rises accordingly.
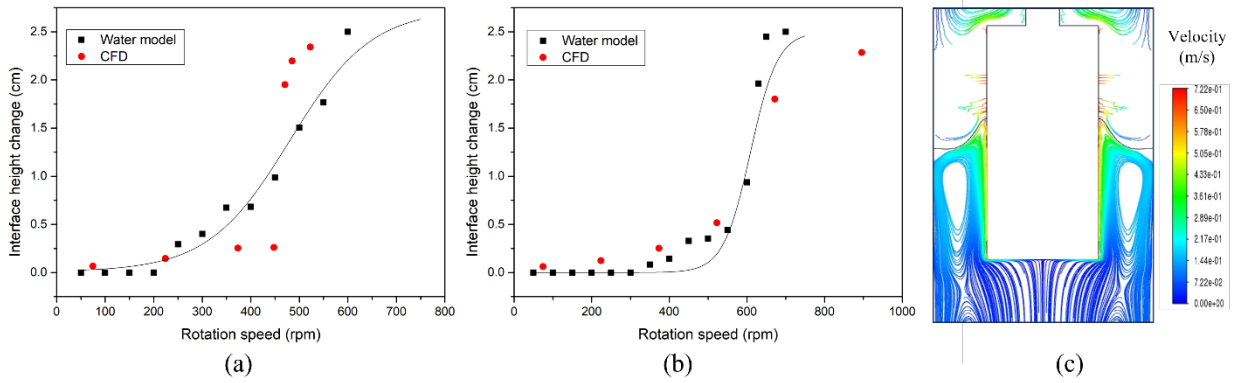
FIG 4 – (a) plot illustrating interface height variation with rotation velocity in experimental and simulated data under 100 cP silicone oil condition, (b) plot illustrating interface height variation with rotation velocity in experimental and simulated data under 1,000 cP silicone oil condition, (c) schematic displaying velocity distribution with colour gradient under the condition of 1,000 cP viscosity for silicone oil at 525 rpm

In industrial conditions, such as ladles containing molten steel and slag, there exists a notable density difference between the two liquids. To consider the effect of density difference, the density ratio is defined by equation (6).

$$\rho_{ratio} = \rho_{silicone\ oil}/\rho_{water} \text{----- (6)}$$

Figure 5(a) compares density ratios of 0.5 and 0.97 at a fixed viscosity of 100 cP in both cases. Below 400 rpm, the similar results is observed between the two conditions. However, above 500 rpm, significant interface movement is evident at a density ratio of 0.97, while less movement is evident at a ratio of 0.5.

Figure 5(b) depicts a schematic of liquid flow under conditions of density ratio 0.50 at 525 rpm. While the velocity distribution resembles that of Figure 4(c), convection of the silicone oil near the silicone oil/water interface is evident, suppressing interface movement. Consequently, insufficient force is exerted to raise the silicone oil/water/refractory interface compared to the case with a higher density ratio.
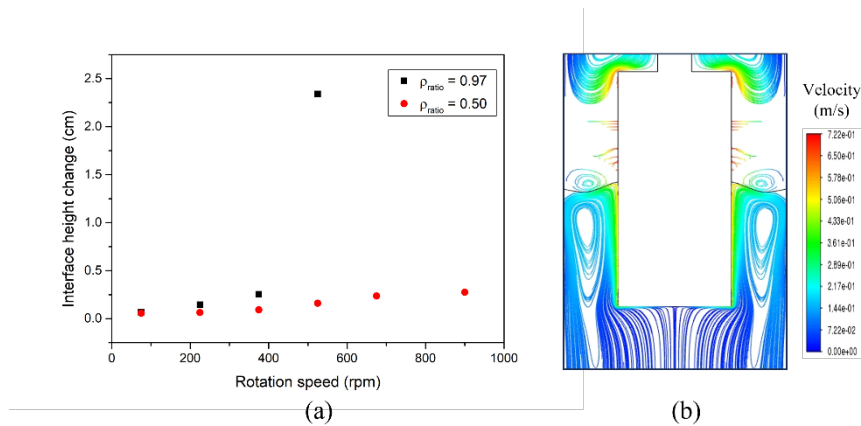
FIG 5 – (a) plot depicting difference in interface height variation based on density ratio, (b) schematic displaying velocity distribution with colour gradient under the condition of density ratio 0.50 and 1,000 cP viscosity for silicone oil at 525 rpm.

Under actual steelmaking conditions involving liquid molten steel and slag, density difference exist. Computational simulations indicate that simulation accuracy is accurate under conditions of significant high-density ratio. Therefore, it is worth considering additional variables such as interfacial tension and contact angle.

6

CONCLUSIONS

This study analysed fluid flow using both water/silicone oil experimental modelling and computational fluid dynamics (CFD) simulations to discern the factors influencing interfacial movement in the two-phase Finger Refractory Test (FRT) experiment involving molten steel and slag.

1. In the water/silicone oil experimental model, the interface rose at rotational velocities of 200 rpm or higher under 100 cP conditions and at 300 rpm or higher under 1,000 cP conditions. Furthermore, as rotational speed increased, the interface movement also increased.

2. During computer simulations utilizing Volume of Fluid (VOF), Multiple Reference Frames (MRF), and Realizable k-epsilon (k-ε) models, similar trends were observed in the water/silicone oil experiment. Water with low viscosity led to interface movement.

3. In simulations comparing density ratio as a variable (0.97 and 0.5), reduced interfacial movement was noted with decreasing density ratio. To accurately simulate the fluid interaction in real operational conditions, additional factors such as interfacial tension or contact angle warrant consideration.

REFERENCES

1. Z. Liu, J. Yu, X. Wang, P. Ma, W. Gu, J. Wen, S. Wei, X. Zhnag, Z. Yan, T. Wen, L. Yuan, and B. Ma. Comparative study of B4C, Mg2B2O5, and ZrB2 powder additions on the mechanical properties, oxidation, and slag corrosion resistance of MgO–C refractories. *Ceramics International* 48.10 (2022): 14117-14126.
2. Y. Liu, Q. Wang, G. Li, J. Zhang, W. Yan, and A. Huang. Role of graphite on the corrosion resistance improvement of MgO–C bricks to MnO-rich slag. *Ceramics International* 46.6 (2020): 7517-7522.
3. P. Zhang and S. Seetharaman. Dissolution of MgO in CaO–"FeO"–CaF2–SiO2 slags under static conditions. *Journal of the american ceramic society* 77.4 (1994): 970-976.
4. W.E. Lee and S. Zhang. Melt corrosion of oxide and oxide–carbon refractories. *International materials reviews* 44.3 (1999): 77-104.
5. R.C.E. Sniezek and J. Szczerba. Corrosion tests for refractory materials intended for the steel industry—A review. *Ceramics-Silikáty* 64.3 (2020): 278-88.
6. Q. Wang, C. Liu, L. Pan, Z. He, G. Li, and Q. Wang. Numerical understanding on refractory flow-induced erosion and reaction-induced corrosion patterns in ladle refining process. *Metallurgical and Materials Transactions B* 53.3 (2022): 1617-1630.
7. K. Cui, J. Wang, H. Wang, Y. Zhang, and T. Fu. Erosion behavior and longevity technologies of refractory linings in blast furnaces for ironmaking: a review. *steel research international* 93.11 (2022): 2200266.
8. S. Zhang and W. E. Lee. Use of phase diagrams in studies of refractories corrosion. *International Materials Reviews* 45.2 (2000): 41-58.
9. E. Benavidez, E. Brandaleze, L. Musante, and P. Galliano. Corrosion study of MgO-C bricks in contact with a steelmaking slag. *Procedia Materials Science* 8 (2015): 228-235.
10. M. Bavand-Vandchali, F. Golestani-Fard, H. Sarpoolaky, H.R. Rezaie, and C.G. Aneziris. The influence of in situ spinel formation on microstructure and phase evolution of MgO–C refractories. *Journal of the European Ceramic Society* 28.3 (2008): 563-569.
11. M. Guo, S. Parada, P.T. Jones, E. Boydens, J.V. Dyck, B. Blanpain, and P. Wollants. Interaction of Al2O3-rich slag with MgO–C refractories during VOD refining—MgO and spinel layer formation at the slag/refractory interface. *Journal of the European ceramic society* 29.6 (2009): 1053-1060.
12. H. Um, K. Lee, K.Y. Kim, G. Shin, and Y. Chung. Effect of carbon content of ferromanganese alloy on corrosion behaviour of MgO–C refractory. *Ironmaking & Steelmaking* 41.1 (2014):

    31-37.

13. J. Jeon, Y. Kang, J. H. Park, and Y. Chung. Corrosion-erosion behavior of MgAl2O4 spinel refractory in contact with high MnO slag. *CeramicP International* 43.17 (2017): 15074-15079.
14. G. J. H. Harmuth and S. Vollmann. Application of an improved testing device for the study of alumina dissolution in silicate slag. *Journal of the European Ceramic Society* 42.8 (2022): 3652-3659.
15. P. Jürgen and C. Brüggmann. Premature wear of refractories due to Marangoni-convection. *steel research international* 83.7 (2012): 637-644.
16. H. Harald and S. Vollmann. Determining the critical Reynolds number for suppressing Marangoni convection of alumina in silicate melt. *Ceramics International* (2024).
17. U. Hyungsic. Corrosion behavior of MgO-C Refractory in contact with ferromanganese slags and/or alloys. *Tech University of Korea master's thesis* (2012): 44-45
18. G.S. Beavers, and D.D. Joseph. Novel Weissenberg effects (1977): 11-19
19. V. Chauhan and S.S. Yadav. Numerical Simulation of Rod Climbing Effect of Newtonian Fluids. *Conference on Fluid Mechanics and Fluid Power*, 2021.
20. D. Bonn, M. Kobylko, S. Bohn, J. Meunier, A. Morozov, and W. Saarloos. Rod-climbing effect in Newtonian fluids *Physical review letters* 93.21 (2004): 214503.
21. T.H. Shih, W.W. Liou, A. Shabbir, Z. Yang, and J. Zhu. A new k-ε eddy viscosity model for high Reynolds number turbulent flows. *Computers & fluids* 24.3 (1995): 227-238.
22. A.E. Ismail, G.S. Grest, M.J. Stevens, D.R. Heine, and M. Tsige. Interfacial structure and dynamics of siloxane systems: PDMS− vapor and PDMS− water. *Macromolecules* 42.8 (2009): 3186-3194.